Directional thermal channeling: A phenomenon triggered by tight packing of heat sources

Hossein Honarvar[a,b,c,d], Joshua L. Knobloch[a,b,c], Travis D. Frazer[a,b,c], Begoña Abad[a,b,c], Brendan McBennett[a,b,c], Mahmoud I. Hussein[c,d,1], Henry C. Kapteyn[a,b,c], Margaret M. Murnane[a,b,c,1], and Jorge N. Hernandez-Charpak[a,b,c]

[a]JILA, University of Colorado, Boulder, CO 80309; [b]STROBE NSF Science and Technology Center, University of Colorado, Boulder, CO 80309; [c]Department of Physics, University of Colorado, Boulder, CO 80309; and [d]Ann and H. J. Smead Department of Aerospace Engineering Sciences, University of Colorado, Boulder, CO 80309

Contributed by Margaret Murnane, August 5, 2021 (sent for review May 16, 2021; reviewed by Pramod Reddy and Mona Zebarjadi)

Understanding nanoscale thermal transport is critical for nanoengineered devices such as quantum sensors, thermoelectrics, and nanoelectronics. However, despite overwhelming experimental evidence for nondiffusive heat dissipation from nanoscale heat sources, the underlying mechanisms are still not understood. In this work, we show that for nanoscale heat source spacings that are below the mean free path of the dominant phonons in a substrate, close packing of the heat sources increases in-plane scattering and enhances cross-plane thermal conduction. This leads to directional channeling of thermal transport—a novel phenomenon. By using advanced atomic-level simulations to accurately access the lattice temperature and the phonon scattering and transport properties, we finally explain the counterintuitive experimental observations of enhanced cooling for close-packed heat sources. This represents a distinct fundamental behavior in materials science with far-reaching implications for electronics and future quantum devices.

nanoscale thermal transport | phonon transport | molecular dynamics | thermal channeling | nanoscale heat sources

The ability to fabricate devices in the deep nanoscale regime, with characteristic dimensions below 10 nm, is driving innovation in energy, nano, and quantum devices. At these scales, the emergence of new behaviors due to the influence of interfaces and geometry give rise to novel material properties that represent unprecedented technological opportunities. The resulting emergent properties can be harnessed for quantum technologies (1), ultralight and strong materials (2), and high-efficiency thermoelectric materials (3–6). However, for realizing the full promise of nanoscale functional engineering better predictive models and characterization techniques are critical. In particular, although efficient thermal management is essential for the smart design of nanodevices (7, 8), a fundamental and predictive understanding of nanoscale thermal transport is still elusive.

For nearly three decades, experimental and theoretical efforts in nanoscale thermal transport (9–14) have revealed unexpected behaviors, particularly in dielectric and semiconductor materials, where phonons are the dominant heat carriers. These nanoscale behaviors appear as deviations from Fourier's law of heat diffusion, which accurately describes thermal transport at the macro scale. Heat diffusion relies on the fundamental assumption that a local thermal equilibrium (temperature) is established through sufficient phonon–phonon scattering events. When the characteristic dimensions of a system approach the average phonon mean free path (MFP), the notion of a local thermal equilibrium is ill-defined, and as a result a diffusion model fails to accurately predict the thermal transport rate (9). Since phonon MFPs relevant to heat flow can range from tens of nanometers up to several microns in materials such as silicon at room temperature (15), the inability to accurately describe thermal transport precludes optimal thermal design and management of a broad range of nanodevices.

Recent experiments have demonstrated that a nanoheater distribution with either size or period on the order of the dominant phonon MFPs can lead to nondiffusive thermal transport, even when patterned on a bulk substrate. Nanoheaters are normally created by heated nanostructures or laser hot spots. When nanoheater sizes are on the order of the phonon MFPs of the substrate, phonons travel away from nanoheaters with fewer scattering events, depositing their energy nonlocally—thus prohibiting diffusive heat flow (10–13, 16–22). Observations of nondiffusive thermal transport away from nanoheaters have been reported using different experimental techniques for both one-dimensional-confined (nanolines) (11, 13, 18, 21, 22) and two-dimensional-confined (nanocubes) nanoheaters (19). As the size of the nanoheater decreases, nondiffusive transport causes a monotonic reduction in the heat transport efficiency compared with the bulk Fourier prediction (11, 13, 18, 19, 21, 22). In more recent work, however, we have shown that if nanoheater size is held constant while nanoheater spacing is reduced (i.e., nanoheaters are nonisolated), thermal transport partially recovers the diffusive transport efficiency (13, 22). However, no consensus has emerged on the fundamental mechanisms underlying this effect (18, 21).

Despite an increasing body of experimental evidence of nondiffusive heat transfer at the nanoscale, current theoretical frameworks have not been able to uncover the underlying physics. Experimental measurements are often fit using phenomenological models based on Fourier's law of heat diffusion, which obscure the fundamental transport phenomena. Moreover, the Boltzmann transport equation with ab initio calculated parameters—which is viewed as a precise

Significance

A critical factor in determining the achievable speeds and efficiencies of electronic devices is the operating temperature. As modern transistors shrink in size to as small as 5 nm, optimal design for temperature control requires a predictive understanding of nanoscale heat dissipation. In this work, we establish a fundamental microscopic description for thermal transport induced by nanoscale heat sources. We uncover the underlying mechanism that drives the counterintuitive behavior discovered recently via extreme UV scatterometry that nanoscale heat sources cool faster when closely packed than when widely spaced. This finding lays the foundation for better temperature management in modern integrated circuits and future quantum devices.

Author contributions: H.H., M.I.H., H.C.K., M.M.M., and J.N.H.-C. designed the research; H.H. and J.L.K. performed the simulations; H.H., J.L.K., T.D.F., B.A., B.M., M.I.H., H.C.K., M.M.M., and J.N.H.-C. contributed new experimental findings and analytic tools; H.H., J.L.K., T.D.F., B.A., B.M., M.I.H., and J.N.H.-C. analyzed theoretical findings; and H.H., J.L.K., T.D.F., B.A., B.M., M.I.H., H.C.K., M.M.M., and J.N.H.-C. wrote the paper.

Reviewers: P.R., University of Michigan; and M.Z., University of Virginia.

The authors declare no competing interest.

[1]To whom correspondence may be addressed. Email: Margaret.Murnane@colorado.edu or mih@colorado.edu.

This article contains supporting information online at https://www.pnas.org/lookup/suppl/doi:10.1073/pnas.2109056118/-/DCSupplemental.

Published September 27, 2021.

model of phonon dynamics (23–25)—is often prohibitive for complex device-relevant sizes and geometries, due to the high computational cost. The need for tractable mesoscopic transport models, which can be directly compared with experiments, has motivated several alternative approaches that have been successful in capturing some of the reported experimental results, including models based on truncated Levy flights (26, 27), suppression functions (13, 28), relaxons (29), and phonon hydrodynamics (14, 30–34), to name a few. However, these approaches have been unable to provide a complete picture of the underlying nanoheating mechanisms.

In this work, we use nonequilibrium molecular dynamics (MD) simulations (35–37) to reveal a comprehensive microscopic understanding of thermal dissipation away from nanoheaters in device-relevant sizes and geometries. By accessing the temperature, the phonon spectral dispersion, and the phonon thermal conduction with incorporation of atomistically resolved behavior we finally explain counterintuitive experimental observations of enhanced cooling for close-packed nanoheaters (13, 22). With access to the atomistic information, we show that for nanoheater spacings that are below the MFP of the dominant phonons in the substrate, increased in-plane scattering causes an enhanced cross-plane thermal conduction, leading to a directional channeling of thermal transport (Fig. 1). This represents a fundamental behavior in materials physics with far-reaching implications for electronics and future quantum devices.

Results

We simulate a periodic array of heated nanostructures that act as nanoheaters, with period P and line width L placed on top of a silicon film substrate with thickness D as shown in Fig. 1*A* (see *Methods* for more details). By using film substrates with finite thickness we constrain the average phonon MFP in the substrate to be roughly equal to the film thickness (38, 39). This feature allows us to fully explore different nondiffusive thermal transport scenarios in our MD simulations by controlling the phonon MFPs independently from nanoheater line width and period. It is important to realize that the geometry considered in this work, which is relevant to many technological applications, is not a trivial extension of the isotropic nanoheater fully surrounded by a medium (9).

We calculate phonon thermal conduction (see *Methods*) for several periodic nanoheater geometries on films with thicknesses of $D = 9.8$, $D = 29.3$, and $D = 48.9$ nm, as shown in Fig. 1*B*. We perform simulations in geometries with a fixed duty cycle of 50%, where the period P between nanoheaters is set at twice the nanoheater line width L. We vary the line width from a few nanometers ($L = 1.1$ nm, $P = 2.2$ nm) to sizes larger than the film thickness ($L = 106.1$ nm, $P = 212.2$ nm) that are comparable to experimental geometries. As the nanoheater line width is reduced toward the average substrate phonon MFPs (approximately equal to film thickness D) we observe a monotonic reduction of the phonon thermal conduction for the 29.3- and 48.9-nm films compared with the uniform film nanoheater case (dashed line in Fig. 1*B*), consistent with experimental studies of isolated nanoheaters (13, 18, 19, 22). For the 9.8-nm film the values are constant within error bars in this region.

At smaller sizes, once the nanoheater period is smaller than the phonon MFPs the phonon thermal conduction increases, reproducing

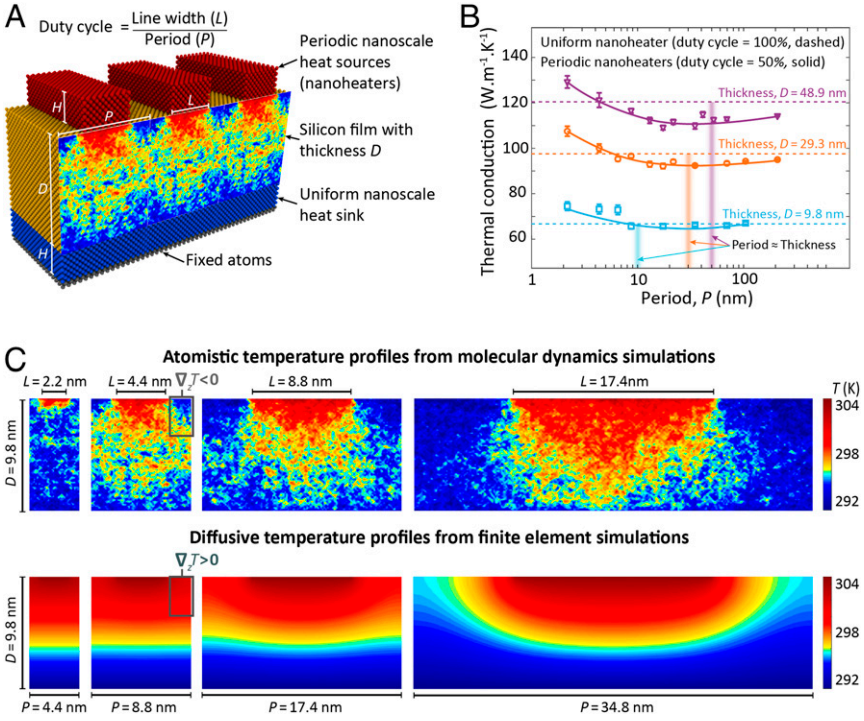

Fig. 1. (*A*) Steady-state MD geometry: periodic silicon nanoheaters of size L and period P on top of a silicon film of thickness D. The color map shows the extracted atomistic temperature profile. (*B*) Cross-plane (downward) phonon thermal conduction plotted as a function of period for three film substrates with thicknesses 9.8, 29.3, and 48.9 nm. The thermal conduction of the corresponding uniformly heated film is shown by dashed horizontal lines. The vertical lines mark the periods that are equal to the thickness of each film. Guides to the eye highlight the trends in the three film substrates; as the nanoheater period (and size) decreases, the cross-plane thermal conduction is reduced compared with the uniformly heated film. However, once the period reaches values on the order of the film substrate thickness this trend reverses. These simulations thus capture the nondiffusive thermal transport behaviors reported experimentally and demonstrate a clear relationship between cross-plane thermal conduction, substrate phonon MFPs, and nanoheater geometry. (*C*) Temperature profiles of periodic nanoheaters with fixed 50% duty cycle for a 9.8-nm-thick film substrate. Atomistic temperature profiles extracted from MD simulations (*Top*) show clear differences compared with diffusive model temperature profiles computed using finite-element analysis simulations (*Bottom*). As the nanoheater size is reduced, the MD simulations show significantly reduced temperatures adjacent to the nanoheaters compared with the diffusive model. These "light bulb"-shaped temperature profiles include negative temperature gradients in the cross-plane direction.

experimental observations of close-packed nanoheaters (13, 22). In extreme nanoscale geometries ($P \approx 2$ to 10 nm depending on the thickness) that have not been experimentally accessible to date, we find a complete return to, or even an apparent exceedance of, the uniform film thermal conduction. We note that the minimum in the thermal conduction trend occurs at a different period P correlating with the film thickness D. Moreover, the magnitude of the deviation from the reference uniform nanoheater increases with increasing film thickness, as also shown in a normalized format in *SI Appendix*, section 1.3. These behaviors are consistent with the expected variation of each system's phonon MFP spectrum, which has been observed to broaden with increasing thickness (38, 39).

The MD simulations give us direct access to the atomistic temperature field in the nanoheaters and films. To compute two-dimensional atomistic temperature profiles, we average the temperature of the atoms in the dimension parallel to the nanoheaters (out-of-plane). In Fig. 1*C*, *Top* we present a selection of atomistic temperature profiles in the 9.8-nm-thick film substrate underneath several nanoheater geometries. For comparison, we show in Fig. 1*C*, *Bottom* the diffusive temperature profiles calculated from finite-element analysis simulations under identical conditions as MD using Fourier's law of heat diffusion (*SI Appendix*, section 1.4). The atomistic and diffusive temperature profiles clearly follow different trends as nanoheater geometry is varied. While the MD and diffusive profiles are similar for large line widths (relative to the phonon MFPs), as the nanoheater geometry is reduced the temperature profiles calculated by MD follow a "light-bulb" shape not observed in the diffusive prediction. This case, shown in the middle two columns, exhibits negative temperature gradients in the cross-plane direction and reduced temperatures compared with the diffusion model results on the surface next to the nanoheaters, as reported in recent experiments (14). Finally, as the nanoheater geometry approaches the extreme nanoscale (left column) the atomistic temperature profile is uniform-like and shows minimal heat deposited in the volume of the film substrate. This behavior for few-nanometer source sizes appears different from both the "light-bulb" shape of intermediate sizes and the diffusive profile. The richness of the atomistic temperature profiles shown in Fig. 1*C* further confirms that using a diffusive model, even with conduction values different from bulk, is insufficient to predict experimental measurements of thermal transport at the nanoscale, as suggested by recent work (14, 27, 40).

Thus far, we have investigated geometries with a fixed duty cycle of 50%, where the period between nanoheaters is set at twice the nanoheater line width. We now compare these results with fixed period geometries, where the period is set to 69.5 nm and only the nanoheater line width is reduced (increasingly isolating the nanoheaters). We term this system the "isolated nanoheater geometry" even though the nanoheaters are periodic, because the interactions of neighboring nanoheaters are reduced. For this comparison, as a case study, we examine nanoheaters on a 29.3-nm-thick film substrate. The resulting cross-plane thermal conduction values, normalized with respect to a uniform nanoheater, versus line width normalized with respect to the average MFP in the film, are shown in Fig. 2*A*.

We investigate the difference between these isolated calculations at fixed period and the close-packed simulations at fixed duty cycle and compare these findings with experimental observations. In the simulations, when the period of the nanoheater distribution is kept constant and the line width is reduced (shown by the blue curve in Fig. 2*A*) we observe a monotonic decrease of the phonon thermal conduction. For these isolated nanoheater calculations we do not observe the turnaround in thermal conduction trend at small line widths (characteristic of the fixed duty cycle case shown as orange curve in Fig. 2*A*). This monotonic behavior in the thermal conduction for nanoheater geometries with fixed period is consistent with many experimental observations (13, 18, 19, 22), and several theoretical frameworks have addressed these deviations from Fourier's law of heat diffusion (18, 19, 31, 33, 41). Moreover, we compare extreme ultraviolet (EUV) scatterometry data, obtained using a high-harmonic laser source with wavelength between l and 40 nm, on bulk silicon (13, 22) with our MD thermal conduction trends. In Fig. 2*B* we plot the inverse of the experimental effective thermal boundary resistivity, normalized with respect to the limiting large-heater resistivity value, and compare it qualitatively with our thermal conduction results. The splitting in the thermal conduction trend between the fixed duty cycle and the isolated nanoheater cases observed in the atomistic computations is in good agreement with the EUV scatterometry data. We note that the EUV scatterometry experiments have line widths, periods, and phonon MFPs that are much larger than in the MD simulations. Nevertheless, once the nanoheater line width is normalized with respect to each system's average phonon MFP the normalized values of thermal conduction and inverse thermal resistivity depend similarly on nanoheater line width. The differences in magnitude between the EUV scatterometry data and MD simulation results are due to the longer MFPs and wider spectrum of the phonons in bulk silicon compared with the silicon film. Additionally, the difference in duty cycle between the EUV scatterometry data (25%) and the MD simulations (50%) does not significantly impact the observed trends. To investigate the fundamental mechanisms that create these nondiffusive transport behaviors we proceed to further analyze the atomistic information provided by MD in wavevector space using spectral energy density (SED) as detailed in *Methods*.

We observe stark differences between the SED of close-packed and isolated nanoheaters. As shown in Fig. 2*C*, for nanoheater line widths below the average phonon MFP the in-plane phonon lifetimes are shorter for close-packed nanoheaters (fixed duty cycle) compared with isolated ones (fixed period). Therefore, in-plane phonon lifetimes decrease with decreasing nanoheater period while the line width is kept constant. Moreover, isolated nanoheaters with 8.8-nm line width and 69.5-nm period have larger in-plane phonon lifetimes, and MFPs, than wide nanoheaters that approach the uniform nanoheater limit, as shown in *SI Appendix*, section 2.4. From this evidence, we conclude that the presence of neighboring nanoheaters increases the scattering of in-plane phonons, while minimally affecting cross-plane scattering. We note that the alteration to lifetimes is not the only change in SED observed between close-packed and isolated sources. We observe an additional dispersion curve with a lower group velocity than the bulk silicon transverse acoustic (TA) branch for both nanoheater geometries, shown in Fig. 2*C*. The appearance of this surface mode arises from more compliant surface atoms with lower coordination than bulk atoms (42). However, as the free surface (spacing) between the nanoheaters is reduced, a near-surface stiffening effect causes the group velocity of the surface mode to increase and approach the bulk TA branch. This effect is mainly limited to geometries with continuous free surface length of less than 8.8 nm (*SI Appendix*, section 2.5.2). The changes in the phonon lifetimes and group velocities between the close-packed and isolated cases result in different in-plane phonon MFPs, directly correlating with the cross-plane thermal conduction trends.

Discussion

The results described in the previous sections directly show the impact of nanoheater distribution geometry on the temperature (shown in Fig. 1*C*), the thermal conduction (shown in Figs. 1*B* and 2*A*), and the in-plane phonon lifetimes (shown in Fig. 2*C*) in the substrate. To interpret these results, we first consider the case of an isolated nanoheater. When the nanoheater line width is much larger than the average phonon MFP (approximately equal to film thickness $D = 29.3$ nm), phonon–phonon scattering near the nanoheater establishes local thermal gradients, and the thermal transport is successfully described by a bulk diffusive model. However, for a line width much smaller than the average phonon

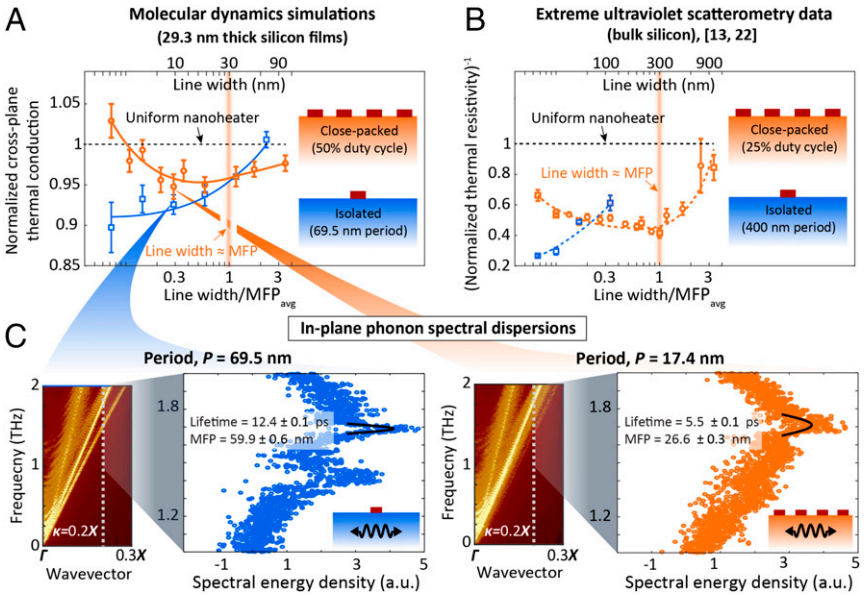

Fig. 2. Phonon thermal transport channeling by periodic nanoheaters. (*A*) Normalized cross-plane thermal conduction in a 29.3-nm-thick silicon film for periodic nanoheaters with fixed duty cycle (orange) and fixed period (blue). The thermal conduction is normalized with respect to the uniformly heated case. (*B*) The inverse of effective thermal boundary resistivity in bulk silicon as measured by ultrafast EUV scatterometry experiments (13, 22), normalized to the value of a large (diffusive) nanoheater. The line width of the nanoheaters in *A* and *B* is normalized to the average phonon MFP in the substrate to account for the differences between the bulk [average phonon MFP ≈ 300 nm (15)] and thin-film silicon MFPs [average phonon MFP is approximately equal to film thickness 29.3 nm (38, 39)]. The qualitative agreement between EUV scatterometry data and the MD simulations is striking. (*C*) In-plane phonon spectral dispersion computed for two geometries with the same line width (8.8 nm) but different period (17.4 nm in orange and 69.5 nm in blue). We extract the lifetimes and MFPs of in-plane phonons by analyzing the phonon spectral dispersion at a particular wavevector. The fit values show that in-plane phonons travel further when nanoheaters are farther apart (blue) than when closer together (orange), as MFP is approximately equal to period. This is direct evidence that increased scattering of in-plane phonons by nearby nanoheaters channels thermal transport to the cross-plane direction, increasing the conduction of the system.

MFP, sharp thermal gradients are produced near the nanoheater's edges as a significant portion of heat-carrying phonons travel ballistically and reduce the density of phonon–phonon scattering near the nanoheater. This behavior is often referred to as "quasiballistic" transport in the literature (11) and can no longer be described by a bulk diffusive model. Our simulations of the small-line-width nanoheater with fixed period (blue in Fig. 2*A*) approximates this isolated case. As shown in *SI Appendix*, section 2.4, we observe that the in-plane phonon lifetimes increase as line width is decreased for an isolated nanoheater. This alteration of the phonon MFPs provides direct evidence of the underlying mechanism behind the experimentally observed decrease in cross-plane thermal conduction as isolated nanoheaters shrink in size below the bulk average phonon MFP [≈300 nm (15)] as shown in Fig. 2*B*.

For close-packed nanoheaters, such as the small-line-width nanoheaters with 50% duty cycle (orange in Fig. 2*A*), neighboring nanoheaters scatter in-plane phonons, reducing their MFP compared with the isolated nanoheater case. With each scattering event involving in-plane phonons that would otherwise travel longer, heat has a chance to travel in a direction other than the in-plane direction, effectively channeling the transport into the cross-plane direction. We refer to this impact of in-plane phonons on cross-plane thermal conduction—which is controlled by nanoheater spacing—as "directional thermal channeling (DTC)." This mechanism is schematically depicted in Fig. 3 and mathematically illustrated in *SI Appendix*, section 4. Therefore, for isolated nanoheaters, the in-plane lifetimes are large, and the cross-plane conduction is small. However, for close-packed nanoheaters, the in-plane lifetimes are small, and the cross-plane conduction is larger. The observed evidence of an in-plane/cross-plane anisotropy in the scattering environment, shown in *SI Appendix*, section 2.3, is consistent with this description.

To check for coherent phonon effects in our analysis we perform additional SED calculations for a third system: isolated nanoheaters surrounded by close-packed unheated nanostructures (nanostructured geometry) as detailed in *SI Appendix*, section 2.5.1. For this system, a fraction of the nanostructures are unheated, unlike the isolated and close-packed geometries where all the nanostructures are heated. From the SED calculations of the nanostructured geometry we observe signatures of Bragg scattering and local resonance only at subwavelength line widths (<10 nm) (5, 6, 37, 43). However, once heat is applied to all nanostructures in this third geometry, the close-packed nanoheaters system is recovered and the coherent phonon dispersion effects are deconstructed (*SI Appendix*, section 2.5.1). Therefore, these coherent phonon effects are not present in the nanoheater geometries presented in Fig. 2. The results of these test cases indicate that Bragg scattering and local resonance effects alone cannot explain our results and that localized heating plays a significant role. Further investigation of

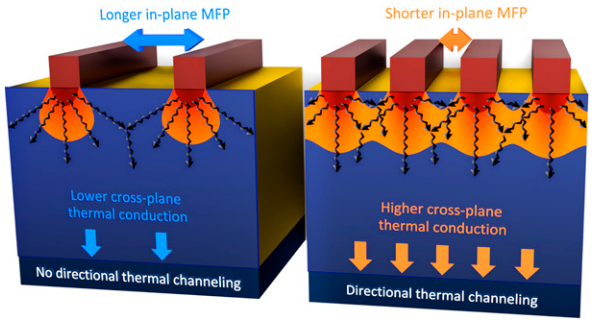

Fig. 3. Microscopic mechanism underlying directional thermal channeling. For close-packed nanoheaters (*Right*), cross-plane thermal conduction is increased due to increased in-plane phonon scattering compared with isolated nanoheaters (*Left*).

the deconstruction of these Bragg scattering and local resonance effects is left to future work.

We further confirm that scattering is the primary mechanism affecting the cross-plane conduction by demonstrating that surface stiffening, which is a linear elastodynamic effect rather than a scattering effect, plays a minimal role in the cross-plane thermal conduction. While surface stiffening appears for the close-packed (orange) geometry in Fig. 2*C*, it is expected to be negligible in an experimental geometry, where the length of the continuous free surface is normally larger (i.e., the lower group velocity branch is always present). In *SI Appendix*, section 3 we verify that surface stiffening is not playing a key role in the thermal conduction trends. We recalculate the thermal conduction values by excluding the surface bin, where the stiffening effect predominantly occurs. The results are similar to those presented for all bins in Fig. 2*A*. Therefore, near-surface stiffening in the top layer dispersion minimally affects the cross-plane conduction.

Finally, our simulations predict that the smallest nanoheater line widths (1.1 to 4.4 nm) will have a cross-plane conduction higher than the uniform nanoheater. At these extremely small sizes, where nanoheaters are 8 to 64 atoms, we suspect that a new transport mechanism may be occurring between the nanoheaters and sink. Further evidence lies in our calculated temperature profiles for the smallest nanoheaters, which show minimal heat deposition in the volume of the film itself (see Fig. 1*C* and more details in *SI Appendix*, section 1.6). Since this exceedance of the uniform nanoheater conduction mainly occurs at sub-10-nm line widths—and it is most pronounced for the 9.8-nm-thick film—we hypothesize that this behavior is related to the wavelength spectrum of the phonons, which ranges in bulk silicon from 1 to 10 nm, with the majority of wavelengths falling below 5 nm (15). At these extremely small scales it is possible that the wavelength distribution of the heat-carrying phonons exiting the nanoheaters is altered. We expect this is a distinct effect from that recently proposed by Chiloyan et al. to occur at larger scales, where higher-than-diffusive conduction can be obtained due to nonthermal phonon populations (44). Further work, both theoretical and experimental, is needed to explore this predicted behavior for sub-10-nm dimensions.

In conclusion, we performed steady-state MD simulations on silicon samples featuring close-packed nanoheaters. We considered device-relevant geometries and used a film substrate to restrict the average phonon MFP and permit a tractable simulation size. These simulations allowed us to access the atomistic information required for directly calculating the temperature field and the phonon dispersion and lifetimes that are difficult to measure experimentally. The simulations reproduce the well-documented experimental behavior that nanoscale heat sources cool faster when closely packed than when widely spaced. This is the case for systems where the total amount of thermal energy applied is the same or even when the thermal energy applied to a closely packed system is higher, as is the case when nanoheaters of the same size are packed closer together. We find that when the line width of a nanoheater is below the MFP of the dominant phonons in the substrate, both the in-plane phonon scattering and cross-plane thermal conduction are enhanced by reducing the spacing between nanoheaters. This indicates a directional channeling and dissipation of thermal transport. These results uncover a mechanistic understanding of phonon transport in silicon and similar materials in the presence of nanoheaters created by heated nanostructures or laser hot spots and finally explain previously reported experimental measurements. Moreover, these findings provide a foundation for developing predictive MD-based models to provide information unattainable by experimental measurements and phenomenological mesoscopic models, which is critically important for the design of optimized nanodevices.

Methods

MD Simulations. Our simulation geometry consists of periodic heated nanostructures with height H on top of a silicon film substrate with thickness D. Under the film substrate we apply a uniform heat sink with the same height as the nanoheaters H to preserve the steady-state condition. At the bottom of the heat sink we have fixed four layers of atoms to maintain the system's stability. Similar to the experimental geometry used in refs. 13 and 22, the nanoheaters and the top surface atoms are free to move. *SI Appendix*, section 1.1 contains more details on the simulation setup.

Thermal Conduction. To characterize the phonon transport in each geometry we extract the temperature gradient and heat flux, as detailed in *SI Appendix*, section 1. From this information, we calculate phonon thermal conduction in the cross-plane direction (downward in Fig. 1*A*) over a linear temperature region of the steady-state profile (*SI Appendix*, section 1.1). We use the term "thermal conduction" mainly because of the finite dimension of the membranes along the cross-plane direction, unlike "thermal conductivity" that is predicted along an infinite dimension such as in a bulk material or in-plane dimensions of a membrane. For reference, we compute the thermal conduction of a system with a uniformly heated film on top of the substrate. The thermal conduction values of the uniformly heated films upon extrapolation to the bulk limit are consistent with the literature (*SI Appendix*, section 1.2) (36).

SED. In our MD simulations we access atomistic information in reciprocal space—primarily phonon anharmonic dispersions—using the SED (37, 43, 45) as described in *SI Appendix*, section 2.1. The SED technique processes the system's atomic velocities by a temporal Fourier transform to obtain an SED magnitude at a specific wavevector. By performing the SED calculation for a set of wavevector points, we extract the phonon anharmonic dispersion, along with phonon properties such as the frequency and lifetime. Using the SED approach, we investigate phonon properties in two limiting directions of transport: cross-plane and in-plane as explained in *SI Appendix*, section 2.3. We find that the cross-plane phonon properties for a given film substrate are unchanged by the nanoheater line width and period, as shown in *SI Appendix*, section 2.3. However, the in-plane phonon properties show strong dependence on the nanoheater geometry. This behavior is indicative of an anisotropy in the scattering environment due to periodic nanoheaters. To investigate the in-plane dependence of the phonon properties further, we divide the substrate into six vertically stacked bins and perform SED calculations for each bin. We find that the phonon properties, and in particular the phonon lifetimes, are most geometry-dependent in the bin closest to the surface, with significantly fewer changes in other bins. Therefore, we focus our calculations on the upper one-sixth of the film substrate. SED dispersions for the other bins can be found in *SI Appendix*, section 2.2.

Data Availability. Some study data are available upon request.

ACKNOWLEDGMENTS. We gratefully acknowledge support from STROBE NSF Science & Technology Center Grant DMR-1548924 and Gordon and Betty Moore Foundation Emergent Phenomena in Quantum Systems (EPiQS) Award GBMF4538. J.L.K. acknowledges support from a Semiconductor Research Corporation Fellowship. This work utilized resources from the University of Colorado Boulder Research Computing Group, which is supported by the NSF (Awards ACI-1532235 and ACI-1532236), the University of Colorado Boulder, and Colorado State University. We also used the Extreme Science and Engineering Discovery Environment, which is supported by NSF Grant ACI-1548562.

1. N. I. Zheludev, Applied physics. The road ahead for metamaterials. *Science* **328**, 582–583 (2010).
2. L. R. Meza, S. Das, J. R. Greer, Strong, lightweight, and recoverable three-dimensional ceramic nanolattices. *Science* **345**, 1322–1326 (2014).
3. J. K. Yu, S. Mitrovic, D. Tham, J. Varghese, J. R. Heath, Reduction of thermal conductivity in phononic nanomesh structures. *Nat. Nanotechnol.* **5**, 718–721 (2010).
4. L. Yang, N. Yang, B. Li, Extreme low thermal conductivity in nanoscale 3D Si phononic crystal with spherical pores. *Nano Lett.* **14**, 1734–1738 (2014).
5. B. L. Davis, M. I. Hussein, Nanophononic metamaterial: Thermal conductivity reduction by local resonance. *Phys. Rev. Lett.* **112**, 055505 (2014).
6. M. I. Hussein, C. N. Tsai, H. Honarvar, Thermal conductivity reduction in a nanophononic metamaterial versus a nanophononic crystal: A review and comparative analysis. *Adv. Funct. Mater.* **30**, 1906718 (2020).
7. M. M. Waldrop, The chips are down for Moore's law. *Nature* **530**, 144–147 (2016).
8. C. Murray *et al.*, "Basic research needs for microelectronics" (US Department of Energy Office of Science, Washington, DC, 2018).

9. G. Chen, Nonlocal and nonequilibrium heat conduction in the vicinity of nanoparticles. *J. Heat Transfer* **118**, 539–545 (1996).
10. Y. K. Koh, D. G. Cahill, Frequency dependence of the thermal conductivity of semiconductor alloys. *Phys. Rev. B* **76**, 075207 (2007).
11. M. E. Siemens *et al*., Quasi-ballistic thermal transport from nanoscale interfaces observed using ultrafast coherent soft X-ray beams. *Nat. Mater.* **9**, 26–30 (2010).
12. J. A. Johnson *et al*., Direct measurement of room-temperature nondiffusive thermal transport over micron distances in a silicon membrane. *Phys. Rev. Lett.* **110**, 025901 (2013).
13. K. M. Hoogeboom-Pot *et al*., A new regime of nanoscale thermal transport: Collective diffusion increases dissipation efficiency. *Proc. Natl. Acad. Sci. U.S.A.* **112**, 4846–4851 (2015).
14. A. Ziabari *et al*., Full-field thermal imaging of quasiballistic crosstalk reduction in nanoscale devices. *Nat. Commun.* **9**, 255 (2018).
15. K. Esfarjani, G. Chen, H. T. Stokes, Heat transport in silicon from first-principles calculations. *Phys. Rev. B* **84**, 085204 (2011).
16. A. J. Minnich *et al*., Thermal conductivity spectroscopy technique to measure phonon mean free paths. *Phys. Rev. Lett.* **107**, 095901 (2011).
17. R. B. Wilson, D. G. Cahill, Anisotropic failure of Fourier theory in time-domain thermoreflectance experiments. *Nat. Commun.* **5**, 5075 (2014).
18. L. Zeng *et al*., Measuring phonon mean free path distributions by probing quasiballistic phonon transport in grating nanostructures. *Sci. Rep.* **5**, 17131 (2015).
19. Y. Hu, L. Zeng, A. J. Minnich, M. S. Dresselhaus, G. Chen, Spectral mapping of thermal conductivity through nanoscale ballistic transport. *Nat. Nanotechnol.* **10**, 701–706 (2015).
20. T. Oyake, M. Sakata, J. Shiomi, Nanoscale thermal conductivity spectroscopy by using gold nano-islands heat absorbers. *Appl. Phys. Lett.* **106**, 073102 (2015).
21. X. Chen, C. Hua, H. Zhang, N. K. Ravichandran, A. J. Minnich, Quasiballistic thermal transport from nanoscale heaters and the role of the spatial frequency. *Phys. Rev. Appl.* **10**, 054068 (2018).
22. T. D. Frazer *et al*., Engineering nanoscale thermal transport: Size- and spacing-dependent cooling of nanostructures. *Phys. Rev. Appl.* **11**, 024042 (2019).
23. D. A. Broido, M. Malorny, G. Birner, N. Mingo, D. A. Stewart, Intrinsic lattice thermal conductivity of semiconductors from first principles. *Appl. Phys. Lett.* **91**, 231922 (2007).
24. W. Li, J. Carrete, N. A. Katcho, N. Mingo, ShengBTE: A solver of the Boltzmann transport equation for phonons. *Comput. Phys. Commun.* **185**, 1747–1758 (2014).
25. J. Carrete *et al*., almaBTE: A solver of the space-time dependent Boltzmann transport equation for phonons in structured materials. *Comput. Phys. Commun.* **220**, 351–362 (2017).
26. B. Vermeersch, J. Carrete, N. Mingo, A. Shakouri, Superdiffusive heat conduction in semiconductor alloys. I. Theoretical foundations. *Phys. Rev. B* **91**, 085202 (2015).
27. B. Vermeersch, A. M. S. Mohammed, G. Pernot, Y. R. Koh, A. Shakouri, Superdiffusive heat conduction in semiconductor alloys. II. Truncated Levy formalism for experimental analysis. *Phys. Rev. B* **91**, 085203 (2015).
28. K. C. Collins *et al*., Non-diffusive relaxation of a transient thermal grating analyzed with the Boltzmann transport equation. *J. Appl. Phys.* **114**, 104302 (2013).
29. A. Cepellotti, N. Marzari, Thermal transport in crystals as a kinetic theory of relaxons. *Phys. Rev. X* **6**, 041013 (2016).
30. S. Lee, D. Broido, K. Esfarjani, G. Chen, Hydrodynamic phonon transport in suspended graphene. *Nat. Commun.* **6**, 6290 (2015).
31. Z. Qu, D. Wang, Y. Ma, Nondiffusive thermal transport and prediction of the breakdown of Fourier's law in nanograting experiments. *AIP Adv.* **7**, 015108 (2017).
32. Y. Guo, M. Wang, Phonon hydrodynamics for nanoscale heat transport at ordinary temperatures. *Phys. Rev. B* **97**, 035421 (2018).
33. P. Torres *et al*., Emergence of hydrodynamic heat transport in semiconductors at the nanoscale. *Phys. Rev. Mater.* **2**, 076001 (2018).
34. M. Simoncelli, N. Marzari, A. Cepellotti, Generalization of Fourier's law into viscous heat equations. *Phys. Rev. X* **10**, 011019 (2020).
35. P. K. Schelling, S. R. Phillpot, P. Keblinski, Comparison of atomic-level simulation methods for computing thermal conductivity. *Phys. Rev. B* **65**, (2002).
36. D. P. Sellan, E. S. Landry, J. E. Turney, A. J. McGaughey, C. H. Amon, Size effects in molecular dynamics thermal conductivity predictions. *Phys. Rev. B* **81**, 214305 (2010).
37. H. Honarvar, M. I. Hussein, Two orders of magnitude reduction in silicon membrane thermal conductivity by resonance hybridizations. *Phys. Rev. B* **97**, 195413 (2018).
38. W. J. Liu, M. Asheghi, Phonon–boundary scattering in ultrathin single-crystal silicon layers. *Appl. Phys. Lett.* **84**, 3819 (2004).
39. X. Wang, B. Huang, Computational study of in-plane phonon transport in Si thin films. *Sci. Rep.* **4**, 6399 (2014).
40. B. Vermeersch, N. Mingo, Quasiballistic heat removal from small sources studied from first principles. *Phys. Rev. B* **97**, 045205 (2018).
41. C. Hua, A. J. Minnich, Heat dissipation in the quasiballistic regime studied using the Boltzmann equation in the spatial frequency domain. *Phys. Rev. B* **97**, 014307 (2018).
42. R. E. Miller, V. B. Shenoy, Size-dependent elastic properties of nanosized structural elements. *Nanotechnology* **11**, 139–147 (2000).
43. H. Honarvar, M. I. Hussein, Spectral energy analysis of locally resonant nanophononic metamaterials by molecular simulations. *Phys. Rev. B* **93**, 081412 (2016).
44. V. Chiloyan, S. Huberman, A. A. Maznev, K. A. Nelson, G. Chen, Thermal transport exceeding bulk heat conduction due to nonthermal micro/nanoscale phonon populations. *Appl. Phys. Lett.* **116**, 163102 (2020).
45. J. A. Thomas, J. E. Turney, R. M. Iutzi, C. H. Amon, A. J. McGaughey, Predicting phonon dispersion relations and lifetimes from the spectral energy density. *Phys. Rev. B* **81**, 081411 (2010).